Tectonophysics 465 (2009) 190–203

Contents lists available at ScienceDirect

Tectonophysics

journal homepage: www.elsevier.com/locate/tecto

Seismic tomography of the Pacific slab edge under Kamchatka

Guoming Jiang [a,b,*], Dapeng Zhao [a], Guibin Zhang [b]

[a] Department of Geophysics, Tohoku University, Sendai 980-8578, Japan
[b] School of Geophysics and Information Technology, China University of Geosciences, Beijing 100083, China

ARTICLE INFO

Article history:
Received 29 April 2008
Received in revised form 20 November 2008
Accepted 25 November 2008
Available online 3 December 2008

Keywords:
Kamchatka
Pacific slab
Slab loss
Arc volcano
Seismic tomography

ABSTRACT

We determine a 3-D P-wave velocity structure of the mantle down to 700 km depth under the Kamchatka peninsula using 678 P-wave arrival times collected from digital seismograms of 75 teleseismic events recorded by 15 portable seismic stations and 1 permanent station in Kamchatka. The subducting Pacific slab is imaged clearly that is visible in the upper mantle and extends below the 660-km discontinuity under southern Kamchatka, while it shortens toward the north and terminates near the Aleutian–Kamchatka junction. Low-velocity anomalies are visible beneath northern Kamchatka and under the junction, which are interpreted as asthenospheric flow. A gap model without remnant slab fragment is proposed to interpret the main feature of high-V anomalies. Combining our tomographic results with other geological and geophysical evidences, we consider that the slab loss may be induced by the friction with surrounding asthenosphere as the Pacific plate rotated clockwise at about 30 Ma ago, and then it was enlarged by the slab-edge pinch-off by the asthenospheric flow and the presence of Meiji seamounts. As a result, the slab loss and the subducted Meiji seamounts have jointly caused the Pacific plate to subduct under Kamchatka with a lower dip angle near the junction, which made the Sheveluch and Klyuchevskoy volcanoes shift westward.

1. Introduction

The Kamchatka peninsula is located at the northwestern edge of the Pacific plate (Fig. 1). The Pacific plate of Cretaceous age subducts beneath the Kamchatka arc and moves along the Bering strike-slip fault at about 8 cm/yr, increasing from 7.7 cm/yr at 55°N to 8.3 cm/yr at 47°N (DeMets et al., 1990; Steblov et al., 2003). Geological studies showed that the volcanism and convergence in Kamchatka ceased at about 55 Ma ago but resumed about 30 Ma ago (Watson and Fujita, 1985). About 10 Ma ago, island-arc magmatism extended to the north of the Aleutian–Kamchatka junction along the mid-Kamchatka volcanic belt, but those are extinct now (Honthaas et al., 1995). A chain of active volcanoes, Holocene in age (Braitseva et al., 1995), along the eastern coast of Kamchatka are underlain by about 100-km depth-contour of the subducting Pacific slab (Gorbatov et al., 1997). The Sheveluch and Klyuchevskoy volcanoes have shifted northwestward from the volcanic front. Between 54°N and 55°N, the Meiji seamounts, the northernmost segment of the Hawaii-Emperor seamount chain, enter the Kamchatka trench (Fig. 1).

The configuration of the Pacific slab under the Kamchatka region was studied by using the distributions of regional earthquakes occurring in the slab, which shows that the dip angle of the slab decreases northward from about 55° to 35° (Gorbatov et al., 1997). The maximum depth of earthquakes becomes shallower along the subduction zone from ~600 km beneath southern Kamchatka to ~100–200 km near the junction (Davaille and Lees, 2004).

Seismic tomography is a powerful tool for determining 3-D velocity structure and dynamic processes in the Earth. Until now several tomographic studies have been performed for the Kamchatka peninsula. Gorbatov et al. (1999) applied the tomographic method of Zhao et al. (1992) to study a 3-D P-wave velocity structure down to a depth of 200 km, and their results showed a prominent low-velocity (low-V) anomaly beneath the volcanic front and a high-velocity (high-V) zone associated with the subducted Pacific slab. But their study region was in the southeastern Kamchatka arc because of the distribution of seismic stations available for them. In order to obtain tomographic images in Northern Pacific, Gorbatov et al. (2000) conducted a regional tomographic inversion and they revealed a slab-like fast anomaly from the Earth's surface down to 900 km depth beneath southern Kamchatka, while a high-V anomaly associated with the Wadati–Benioff zone was not imaged near the junction. A surface-wave tomography shows that the subducting Pacific lithosphere terminates at the Aleutian–Kamchatka junction and no relict slab underlies the extinct northern Kamchatka volcanic arc (Levin et al., 2002a). Although Levin et al. (2002a) suggested two episodes of slab loss under northern Kamchatka, their tomographic images could not reveal the detached slab because their model is limited to 200 km depth. Recently, Lees et al. (2007) determined P-wave teleseismic tomography which showed evidence for slab shoaling toward the

* Corresponding author. School of Geophysics and Information Technology, China University of Geosciences, Beijing 100083, China.
E-mail addresses: jiang_guoming@163.com, gm_jiang2008@yahoo.com.cn (G. Jiang), zhao@aob.geophys.tohoku.ac.jp (D. Zhao).

0040-1951/$ – see front matter © 2008 Elsevier B.V. All rights reserved.
doi:10.1016/j.tecto.2008.11.019

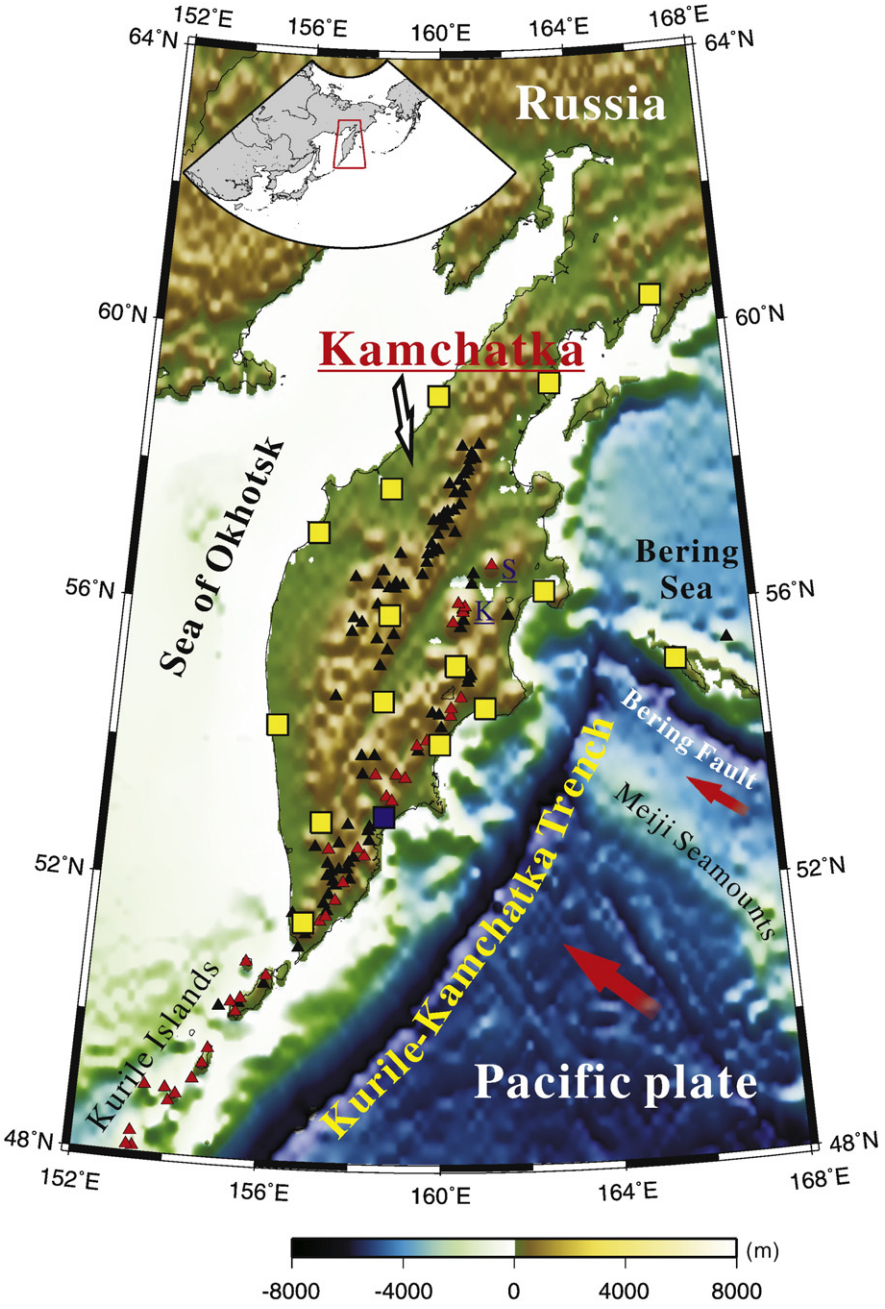

Fig. 1. Map of the study area with surface topography shown in colors (its scale is shown at the bottom). Yellow squares show the locations of 15 portable seismic stations deployed for the SEKS experiment in the Kamchatka region. The blue square denotes a permanent station (PET). Red arrows denote the motion direction of the Pacific plate subducting along the Kurile–Kamchatka trench and transcurrent motion along the Bering Fault. Red and Black triangles represent the active and inactive volcanoes, respectively. S, Sheveluch volcano; K, Klyuchevskoy volcano. The insert map shows the location of the present study area.

northern edge of the subducted Pacific slab, and they considered the thermal ablating related to asthenosphere as a possible cause for the feature.

Shear-wave splitting studies suggested that trench-parallel strain follows the seismogenic Wadati–Benioff zone, but rotates to trench-normal beyond the slab edge (Peyton et al., 2001; Portnyagin et al., 2005), indicating that the asthenospheric flow passes through a slab window beneath the junction, similar to that observed in Apenines (Wortel and Spakman, 2000). In addition, thermal modeling of the reheating of a torn slab shows that the Pacific lithosphere was already thinner well before entering the trench due to delayed thickening of the lithosphere below the Meiji–Hawaiian hotspot (Davaille and Lees, 2004).

In the present study we use teleseismic tomography to determine a 3-D P-wave velocity structure down to 700 km depth under Kamchatka. Our results provide new evidence for the loss of the Pacific slab at the slab edge, which may improve our understanding of the dynamic processes under this region.

2. Data and method

We used teleseismic data recoded by 15 portable broad-band seismic stations in Kamchatka from the SEKS experiment conducted in 1998–1999 (Lees et al., 2000), and by one permanent station PET. Fig. 1 shows the distribution of the 16 seismic stations used. All the waveform data were downloaded from the web site of IRIS

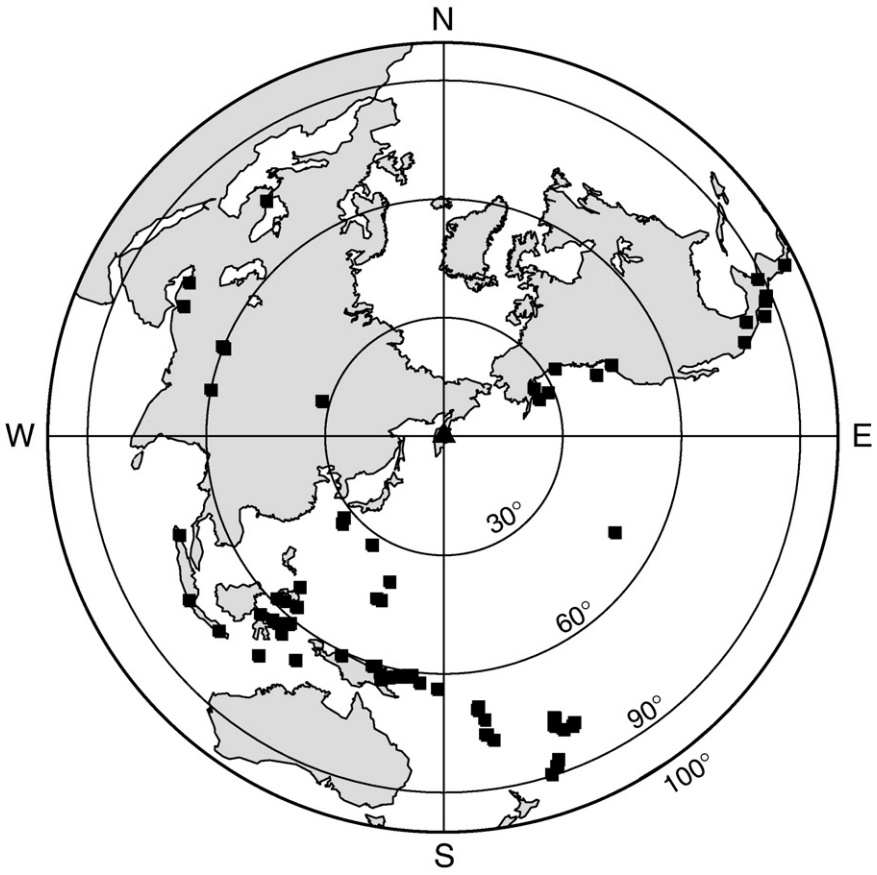

Fig. 2. Epicentral locations of the 75 teleseismic events (squares) used in this study. The triangle denotes the center of Kamchatka.

(Incorporated Research Institutions for Seismology). We selected earthquakes with epicentral distances between 25° and 95° (Fig. 2), which have magnitudes larger than M 5.0 and were recorded by more than 5 stations. The selected events have nearly complete azimuthal coverage except for the regions of the Arctic Ocean and the Atlantic Ocean (Fig. 2). In this work, we picked manually P-wave arrival times from the original seismograms. The picking accuracy is estimated to be 0.1–0.2 s (Fig. 3). As a result, we collected 678 P-wave arrivals from 75 teleseismic events recorded by the 16 seismic stations. The ray paths used in this study crisscross well in both the horizontal and vertical directions down to 700 km depth (Fig. 4).

To determine the 3-D velocity structure under the study area, we adopted an updated version of the tomographic method (Zhao et al., 1994, 2006) to invert relative travel-time residuals of the teleseismic events selected. Theoretical P-wave travel times were calculated by using the iasp91 1-D Earth model (Kennett and Engdahl, 1991). Residuals were obtained by subtracting these theoretical arrival times from the observed ones, and relative residuals were calculated for each event by subtracting its corresponding mean residual from the raw residuals. Distribution of the average relative residuals at each station is shown in Fig. 5a, which reflects the lateral heterogeneity under the seismic network. Large early arrivals at stations on the eastern coast reflect the old and thick Pacific plate subducting beneath the Kamchatka peninsula. Large delayed arrivals are observed at stations both on the western coast and in the northeast and center of Kamchatka, which suggest the existence of significant low-velocity materials beneath that region. Minor early and delayed arrivals at stations PAN, TIG, ESS and APA reflect the complex structural variations under these stations.

A 3-D grid was set up in the study area. Velocity perturbations from the 1-D iasp91 model at the grid nodes were taken as unknown parameters. The velocity perturbation at any point in the model was computed by linearly interpolating the velocity perturbations at the eight grid nodes surrounding that point. A 3-D ray tracing technique was used to compute ray paths and travel times (Zhao et al., 1992). The large and sparse system of observation equations that relate the observed data to the unknown velocity parameters was resolved by using a conjugate-gradient algorithm LSQR (Paige and Saunders, 1982) with damping and smoothing regulations (Zhao, 2001, 2004). The station elevations were taken into account in the 3-D ray tracing and inversion. We selected the optimal damping parameter, 5.0, from detailed analyses of the trade-off between data variance reduction and model smoothness (Fig. 6).

3. Analysis and results

Teleseismic tomography cannot determine the 3-D crustal structure well because the teleseismic rays arrival at stations nearly vertically and so they do not crisscross well near the surface (Fig. 4). Hence, it is necessary to correct the teleseismic relative residuals for the heterogeneous crustal structure (e.g., Lei and Zhao, 2005; Montelli et al., 2006; Zhao et al., 2006). In general, crustal structure can be obtained either from local seismic studies in the study region (using seismic soundings or receiver function method, etc.) or from a global crustal model. In the present study area, 1-D P-velocity crustal models under only 9 stations were estimated by a receiver-function analysis (Levin et al., 2002b). Although Nizkous et al. (2006) determined a more detailed crustal velocity model beneath Kamchatka, their model is not available for all the 16 stations used in our study because their study region is located in southeastern Kamchatka close to the Kurile–Kamchatka trench. Therefore we prefer to use the global crustal model CRUST2.0 (Laske et al.) which is an updated version of CRUST5.1

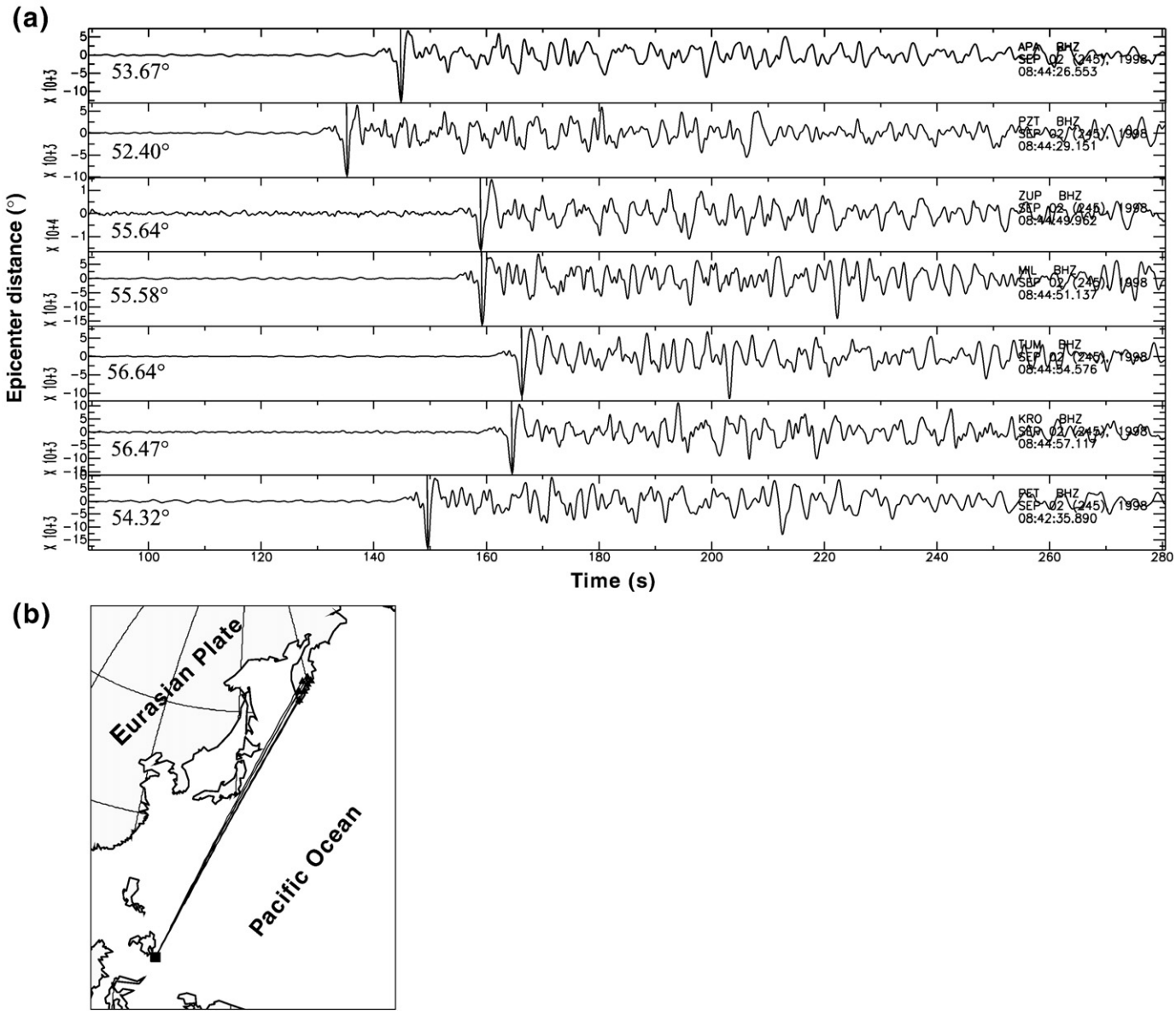

Fig. 3. (a) Seismograms of a teleseismic event with M 6.8 occurred on September 2, 1998 (see (b) for its epicenter location). The vertical lines show the P-wave arrivals we picked manually. The number on the left under each trace represents the epicenter distance in degree. (b) The location of event, stations and corresponding rays. The square and triangles represent the event and the stations, respectively.

(Mooney et al., 1998) and is specified on a 2°×2° grid for the lateral velocity variations of the crust and the Moho topography. The average Moho depth is 35 km in Kamchatka (Gorbatov et al., 1999). Fig. 5b shows the distribution of average relative residuals after the crustal correction. Comparing Fig. 5a with Fig. 5b, we can see that the relative residual at station SBL changes from a delay to an early arrival, which may suggest a low-V structure in the crust beneath this station. In contrast, at station ESS the average residual changes from an early to a delayed arrival, which probably indicates that the velocity is relatively high in the crust but low in the upper mantle beneath this station. The results of the relative residuals are consistent with the receiver function analysis (Levin et al., 2002b).

We performed many tomographic inversions using different grids. The spacing between grid nodes ranges from 1.0 to 3.0° laterally and from 50 to 200 km in depth. Inversions were also performed by using various damping and smoothing parameters. Many checkerboard tests are performed for determining a suitable grid interval. If the grid spacing is too small, the anomalies at the grid nodes could not be restored well because of the insufficient ray coverage and criss-crossing. Comparing all the results using different grids, we found the optimal model with grid nodes at depths of 50, 200, 300, 400, 500, and 700 km, and having a grid interval of 2.0° in the lateral direction (Fig. 7).

Fig. 8 shows the plane views of our optimal tomographic results. There are two prominent features in the image. One is high-V anomalies (about 4%) associated with the subducting Pacific slab under southern Kamchatka. At the shallow depth, the high-V anomaly terminates near the Aleutian–Kamchatka junction (Fig. 8a–b). The high-V anomaly under southern Kamchatka seems truncated to the south perhaps due to the lower resolution there, while a local tomography shows that the slab is continuous there (Gorbatov et al., 1999). As the depth increases, the high-V anomaly shifts from the eastern coast to the western coast (Fig. 8c–e), but extends to the north of Kamchatka behind the junction at 700 km depth (Fig. 8f), which is consistent with the previous tomographic results (Gorbatov et al., 2000; Lees et al., 2007). However, this high-V anomaly is uncertain

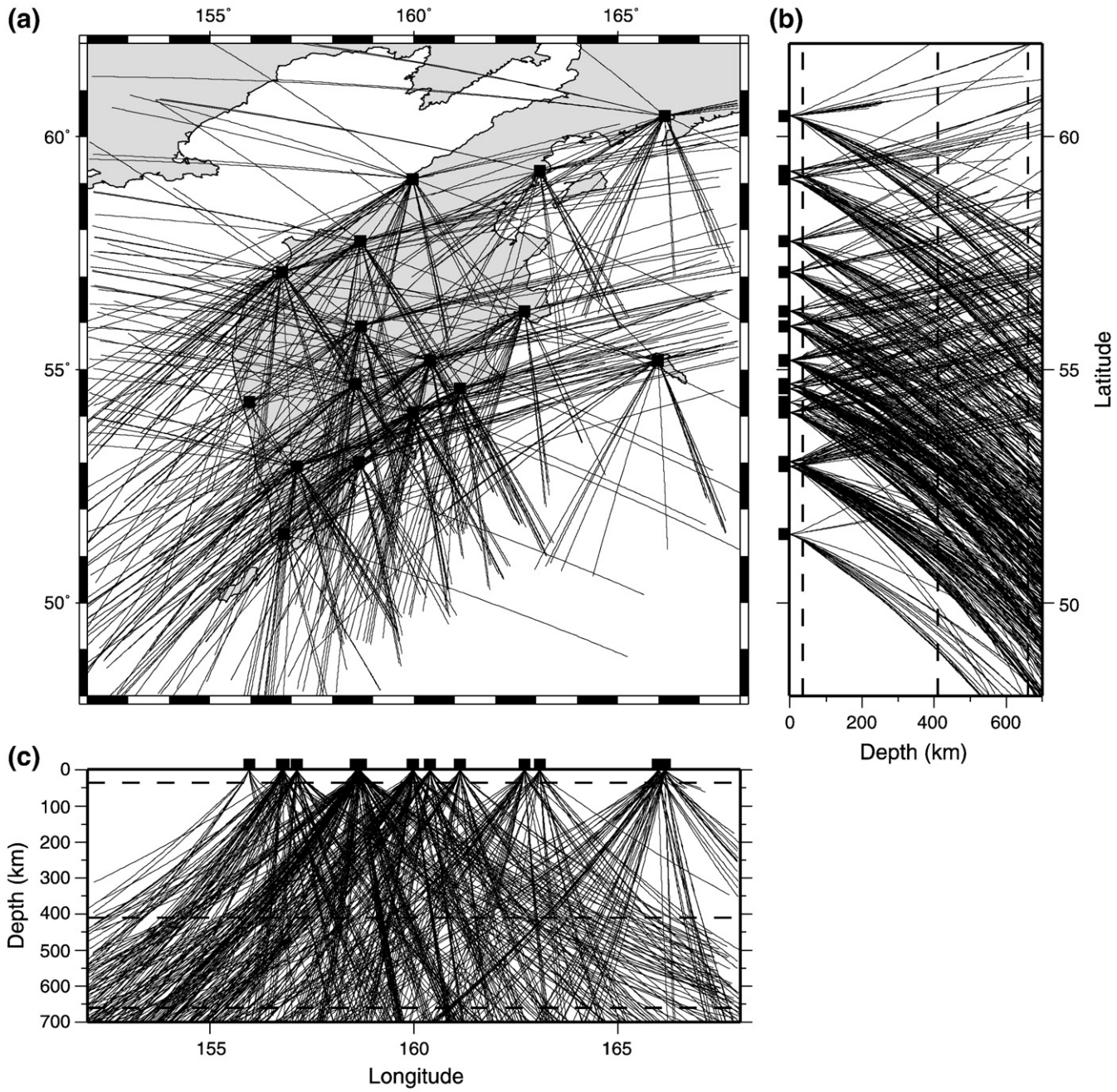

Fig. 4. Distribution of P-wave rays used in this study in plan view (a) and in north–south (b) and east–west (c) vertical cross-sections. Squares denote the 16 seismic stations used. The dashed lines in panels (b) and (c) denote the Moho, 410 and 660 km discontinuities, respectively.

because of the poor ray coverage there. Another prominent feature is that low-V anomalies are visible beneath the junction of the Kurile–Kamchatka trench with the Bering fault (Fig. 8b–d), which may indicate mantle flow passing through the junction, forming a slab window (Peyton et al., 2001). Low-V zones also exist under the volcanic front (Fig. 8a), which represent arc magmas, similar to those in the other subduction zones (e.g., Zhao et al., 1992, 1994). In addition, a clear high-V zone is visible beneath the Bering Sea near the junction (Fig. 8), which may reflect the subducted Pacific plate along the Aleutian trench. However, this feature is still uncertain due to the lower resolution there.

Figs. 10 and 11 show 14 vertical cross-sections of the tomographic images along profiles AA′–NN′, which cover the entire Kamchatka peninsula (Fig. 9). The earthquakes occurring within a width of 30 km and the volcanoes locating within a width of 10 km from a profile are superposed on each cross-section. We obtained the hypocenter parameters of the local earthquakes from two sources. One is downloaded from the IRIS web site. The other is the global earthquake list by Dr. Engdahl (see Engdahl et al., 1998), which is considered to have more accurate hypocenter locations. Profiles AA′–HH′ are normal to the Kurile–Kamchatka trench, while profiles II′–NN′ are perpendicular to the trench (Fig. 10).

Along profile AA′ which is located at the edge of the study area (southern Kamchatka, Fig. 10a), the Wadati–Benioff zone extends down to a depth of about 660 km, however, the high-V slab is visible only down to about 550 km perhaps due to the limitation of the resolution and ray path coverage. Along profiles BB′–DD′, the high-V slab extends well beyond the leading edge of the Wadati–Benioff zone,

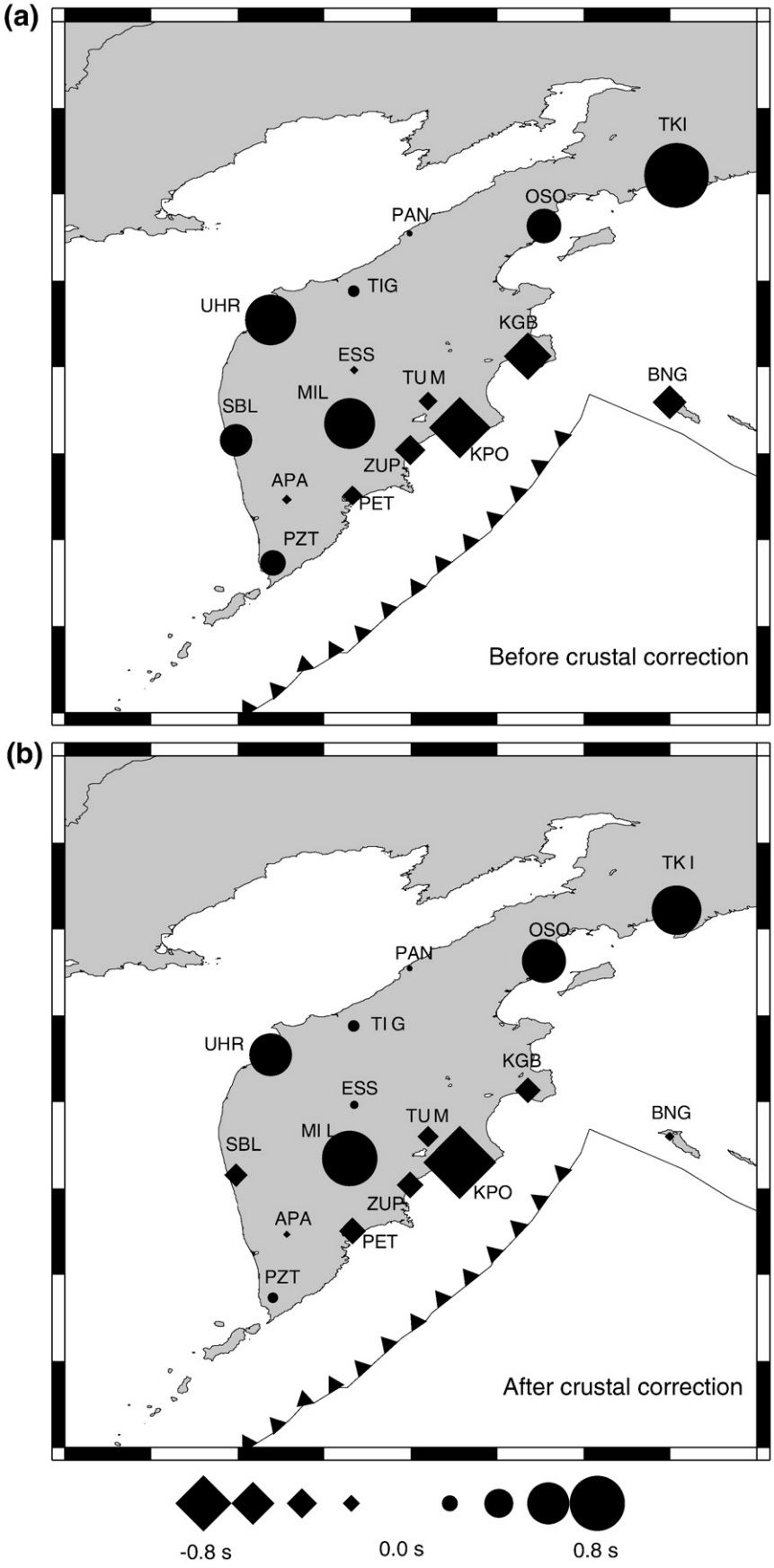

Fig. 5. (a) Distribution of relative travel-time residuals at each of the stations used in this study before making the crustal correction. (b) Distribution of the relative travel-time residuals after the crustal correction by using the CRUST2.0 model (see text for details). Diamond and circle symbols denote early and delayed arrivals, respectively. The scale for the residuals is shown at the bottom. The line with ticks and the thin line represent the Kamchatka trench and the Bering fault, respectively.

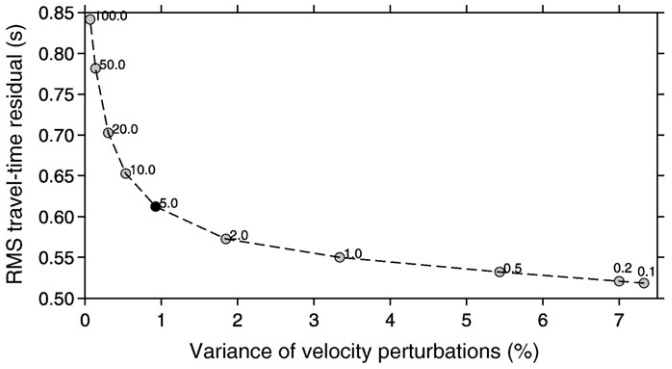

Fig. 6. Trade-off curve between the variance of velocity perturbations and root-mean-square (RMS) travel-time residual of the tomographic inversions with different damping values. The numbers beside the circles denote different damping values from 0.1 to 100.0. The black circle represents the optimal damping value used in this study.

through the transition zone, and may reach a depth of about 900 km (Gorbatov et al., 2000; Lees et al., 2007). Fig. 10d shows a different pattern that the high-V zone seems to be separated near a depth of 400 km without mantle flow passing through the gap where the lithosphere may be heated by the surrounding asthenospheric flow. The upper part of the high-V zone is consistent with the Wadati–Benioff zone (Fig. 10d). Along profiles EE′–HH′ passing through central and northern Kamchatka, the high-V zone is separated into two parts by low-V zones (Fig. 10e–h). The upper part shoals from the central to northern Kamchatka with the same pattern as the Wadati–Benioff zone, while the lower part is visible below 410 km depth. In the GG′ section locating to the north of Sheveluch volcano, the high-V zone associated with the Wadati–Benioff zone becomes too short to be identified as an inclined slab (Fig. 10g), the same as that found by Gorbatov et al. (2000). Furthermore, along profile HH′, there are no distinct high-V zone and the Wadati–Benioff zone, which may indicate the absence of a subducting slab (Fig. 10h). Comparing

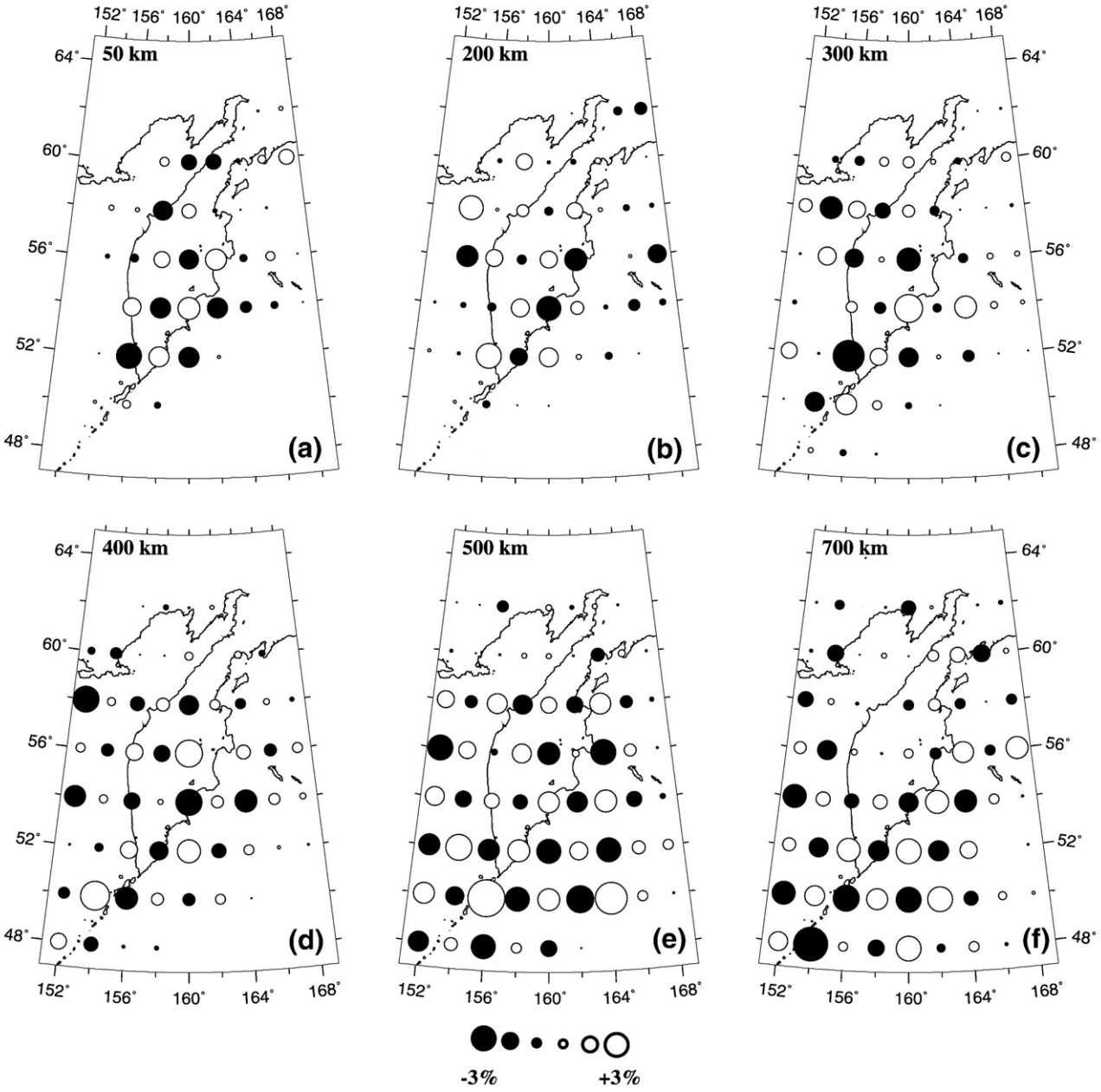

Fig. 7. Results of a checkerboard resolution test. Open and solid circles denote fast and slow velocities, respectively. The velocity perturbation scale is shown at the bottom. The layer depth is shown at the upper-left corner of each map.

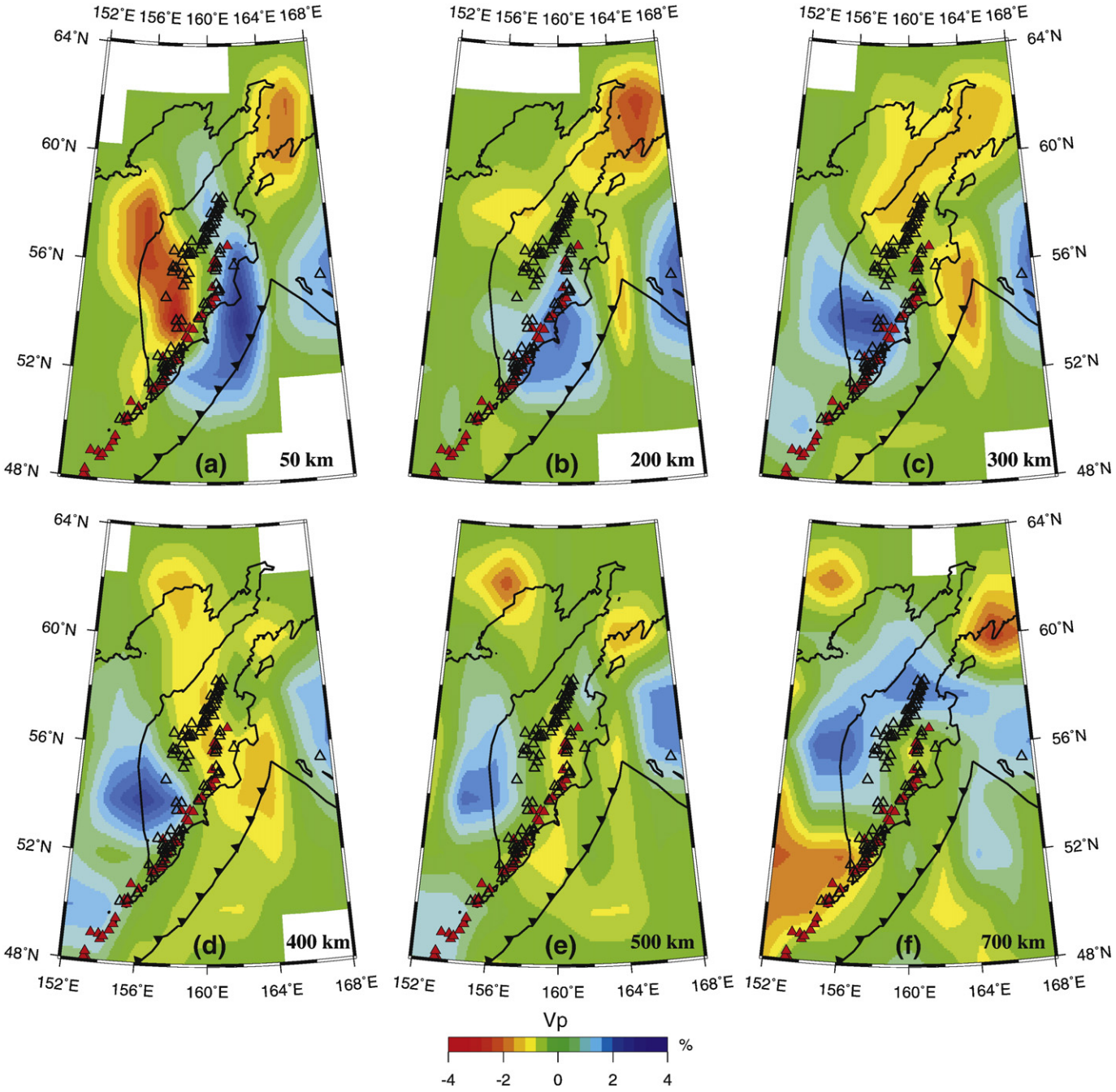

Fig. 8. Plan views of P-wave velocity images obtained in this study. Red and blue colors denote slow and fast velocities, respectively. Open and solid (red) triangles show inactive and active volcanoes, respectively. The depth of each layer is shown at the lower-right corner of each map. The velocity perturbation scale is shown at the bottom.

with the previous tomographic studies (e.g., Lees et al., 2007), we found in this study systematic variations in the morphology of the subducting Pacific slab and its relationship with the Wadati–Benioff deep seismic zone under Kamchatka as shown in many of the cross sections (Figs. 10 and 11).

Fig. 11 shows the cross-sections along profiles II′–NN′ (see Fig. 9 for their locations) which shift from the eastern coast to the western coast. Along profiles II′–KK′, we can see that the high-V zone and the Wadati–Benioff zone are thin and shallow near the junction, while they become thicker and deeper gradually southward. Low-V anomalies exist under the high-V zone (Fig. 11a–c). These features are consistent with the variations in the dip angle (Gorbatov et al., 1997) and thickness of the Pacific slab (Davaille and Lees, 2004). From profiles LL′ to NN′, the seismicity becomes deeper and the high-V zone is mainly visible under Southern Kamchatka and it even extends down to the uppermost part of the lower mantle (Fig. 11d–f).

4. Resolution tests

To confirm the main features of the tomographic result, we conducted detailed resolution analyses. A direct way to evaluate the resolution of a tomographic result is to calculate a set of travel-time delays that result from tracing the corresponding rays through a synthetic structure as though they are data, and then to compare the inversion result with the initial synthetic structure. In the resolution tests, the numbers of stations, events and ray paths are the same as those in the real data set. In this work, we conducted two kinds of

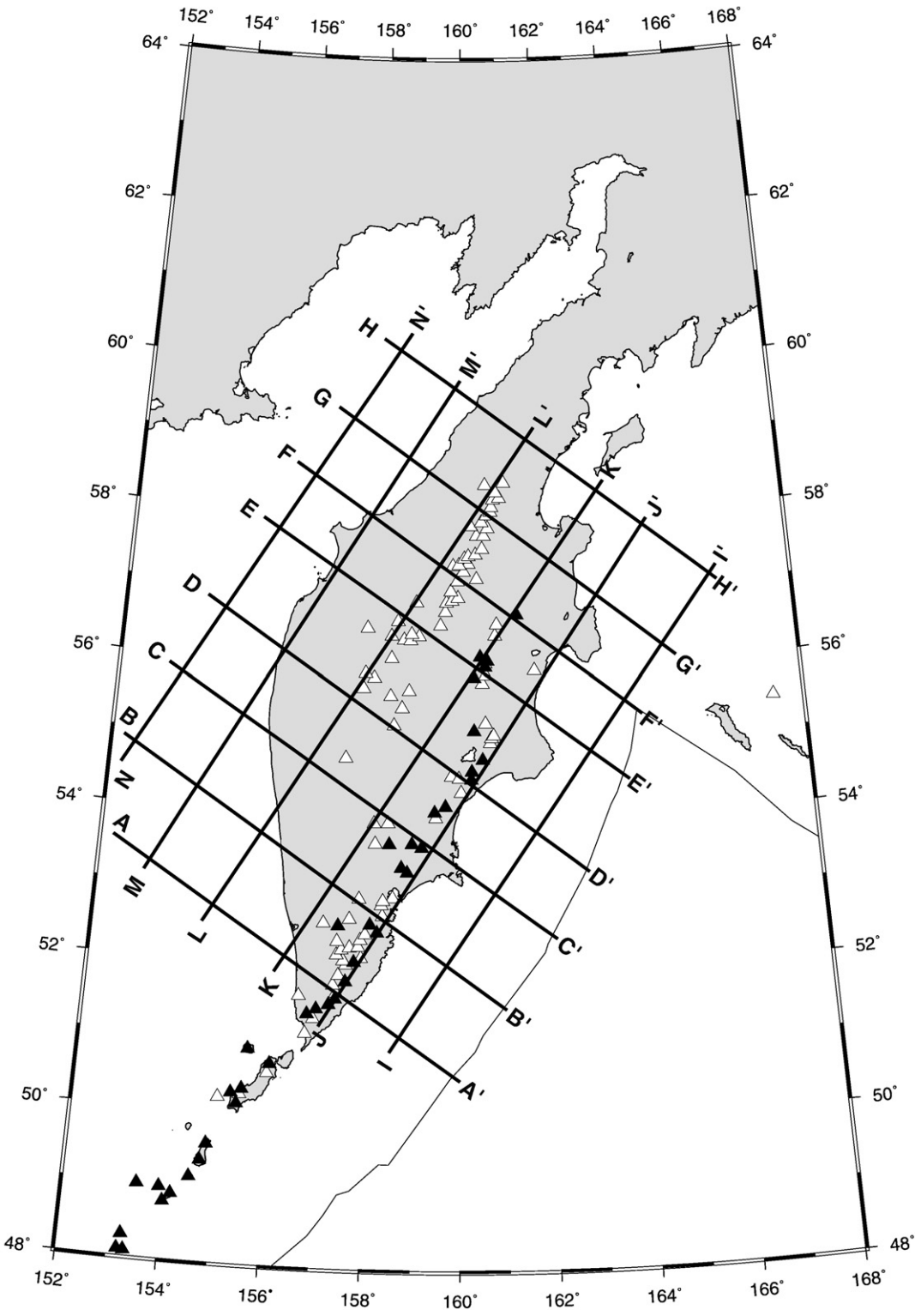

Fig. 9. Locations of the vertical cross sections shown in Figs. 10–12. White and black triangles show inactive and active volcanoes, respectively.

resolution tests. In each test, random errors with a standard deviation of 0.15 s were added to the synthetic data in order to simulate errors contained in the real data set. The first test is a checkerboard resolution test for evaluating the spatial resolution of tomographic images in the entire study area (Humphreys and Clayton, 1988; Zhao et al., 1992). To make a checkerboard, positive and negative 3% velocity perturbations are assigned to the 3-D grid nodes that are arranged in the modeling space, the image of which is straightforward and easy to remember. The grid spacing for the checkerboard test is the same as that for the tomographic inversion of the real data. The test results show that the shallower part (at 50 km depth) of the study area has a lower resolution (Fig. 7a) because the teleseismic rays do not crisscross well near the surface (Fig. 4). The resolution becomes better from 100 to 700 km depth (Fig. 7b–f).

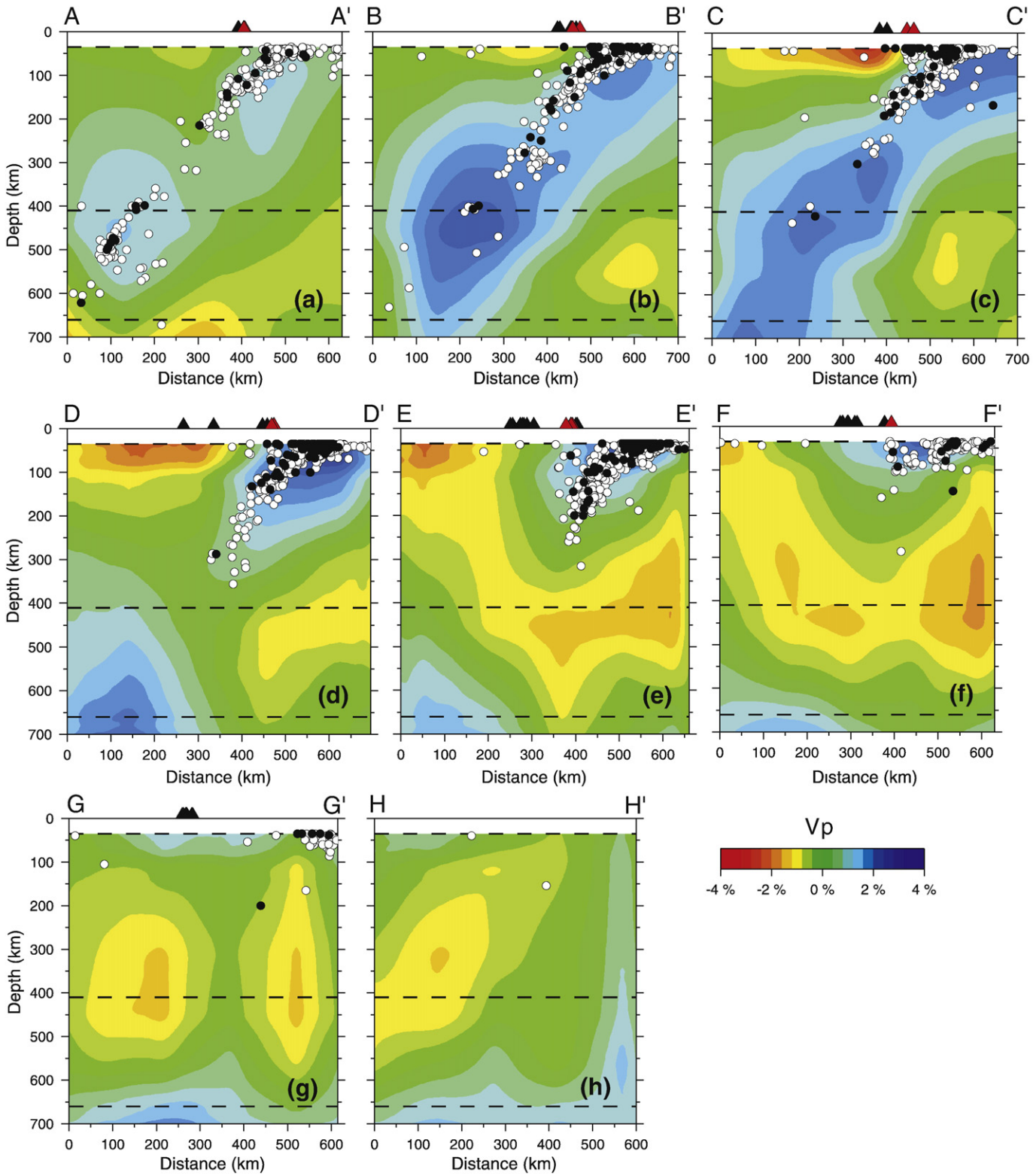

Fig. 10. Vertical cross sections of P-wave velocity images obtained by this study. The locations of the cross sections are shown in Fig. 9. Red and blue colors denote slow and fast velocities, respectively. Black and red triangles denote inactive and active volcanoes within a 30-km width of each profile, respectively. White dots indicate earthquake hypocenters within a 30-km width of each cross section (the hypocenter parameters are obtained from the IRIS web site), while black dots show the earthquake hypocenters relocated by Engdahl et al. (1998) which should be more accurate. The three dashed lines denote the Moho, 410 and 660 km discontinuities, respectively. The velocity perturbation scale is shown at the bottom.

The second test we conducted is a synthetic test for examining the reliability of the high-V slab. The procedure of the synthetic test is similar to that of the checkerboard resolution test. That is, we firstly constructed a synthetic input model including the subducting Pacific slab (Fig. 12a–c), then synthetic data were calculated for the synthetic model using the real locations of earthquakes and stations.

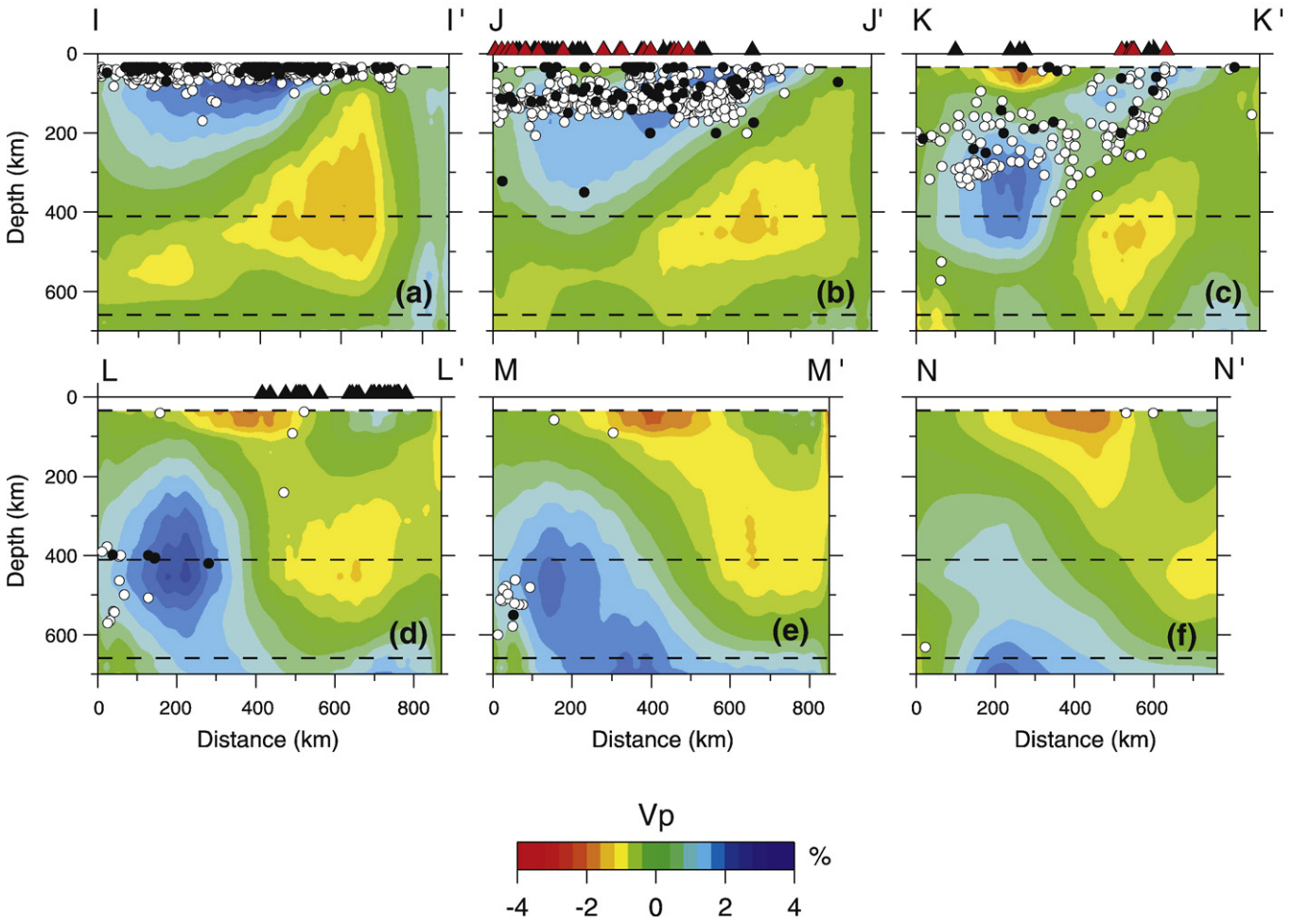

Fig. 11. The same as Fig. 10 but along profiles II′ to NN′ (see Fig. 9 for their locations). The earthquakes (white and black dots) are located within a 20-km width of each profile.

Next the synthetic data were inverted to obtain the output model (Fig. 12d–f). Comparing the input and the output models, we can conclude that the main features of the high-V slab can be recovered very well.

5. Discussion

According to our tomographic results, we proposed a "gap" model to describe the feature of the high-V zone, which extends below the mantle transition zone under southern Kamchatka and shortens gradually northward and ends near the Aleutian–Kamchatka junction (Fig. 13). In this new model, there exists a gap associated with the loss of the subducted lithosphere beneath Sheveluch and Klyuchevskoy volcanoes near the Pacific slab edge. The asthenospheric flow can pass through the gap around the slab edge to the north. This feature of lost slab can also be found at other slab edges, for example, in Apennines (Lucente et al., 1999; Wortel and Spakman, 2000) and in Taiwan (Lallemand et al., 2001). In addition, the subducted lithosphere near the edge is thinner than that under southern Kamchatka due to the Meiji Seamounts subducting together with the Pacific plate. Levin et al. (2002a) presented a detached model to interpret the phenomena of the earthquakes shoaling northeastward. They suggested that a relic slab detached from the westward subduction of the Pacific plate at about 2 Ma ago. Nevertheless, their model does not show how the slab is separated and where the relic slab is. In our model, there is no remnant slab fragment near the edge, which is largely different with that of Levin et al. (2002a), but it is consistent with the results presented by Lees et al. (2007).

What causes the loss of the subducted Pacific slab? Combining our results with the geological, geophysical and geochemical evidences, we consider that the gap has undergone two stages until now. In the first stage, during the Oligocene–Middle Miocene, the Okhotsk Sea had opened as the Kurile trench fell back (Kimura, 1994). The volcanism and convergence in Kamchatka ceased at about 55 Ma ago, but they resumed at about 30 Ma ago. During that period, the Aleutian–Kamchatka junction had located near the southern end of Kamchatka arc, and then has moved to the present position (Gordon and Jurdy, 1986; Bazhenov et al., 1991). During the movement for about 20 million years, the subducted Pacific slab had interacted with the surrounding mantle flow, therefore depleted some lithospheres near the edge due to the thermal friction. As a result, a gap had been generated and enlarged gradually. Unfortunately, there is no other evidence for this process at present. After the slab arrived at the present position, the mantle flow has continued to interact with the edge of the subducted lithosphere. In the second stage, the asthenospheric flow plays a dominating role to pinch off the slab edge. Yogodzinski et al. (2001) suggested the existence of a slab window locating beneath the western Aleutian and the Aleutian–Kamchatka junction. The mantle flow can pass through the window from the Aleutian arc into the Kamchatka peninsula, which is well reflected in our results (Figs. 8b–d and 13) and in a seismic anisotropy study (Peyton et al., 2001). During the convection, the mantle flow has induced partial melts to the slab-edge in the overlying mantle (Park et al., 2002). The adakites have been found in Sheveluch but not in Klyuchevskoy volcano, which strongly indicates that the slab-edge near the junction is molten. In addition, a tank experiment was

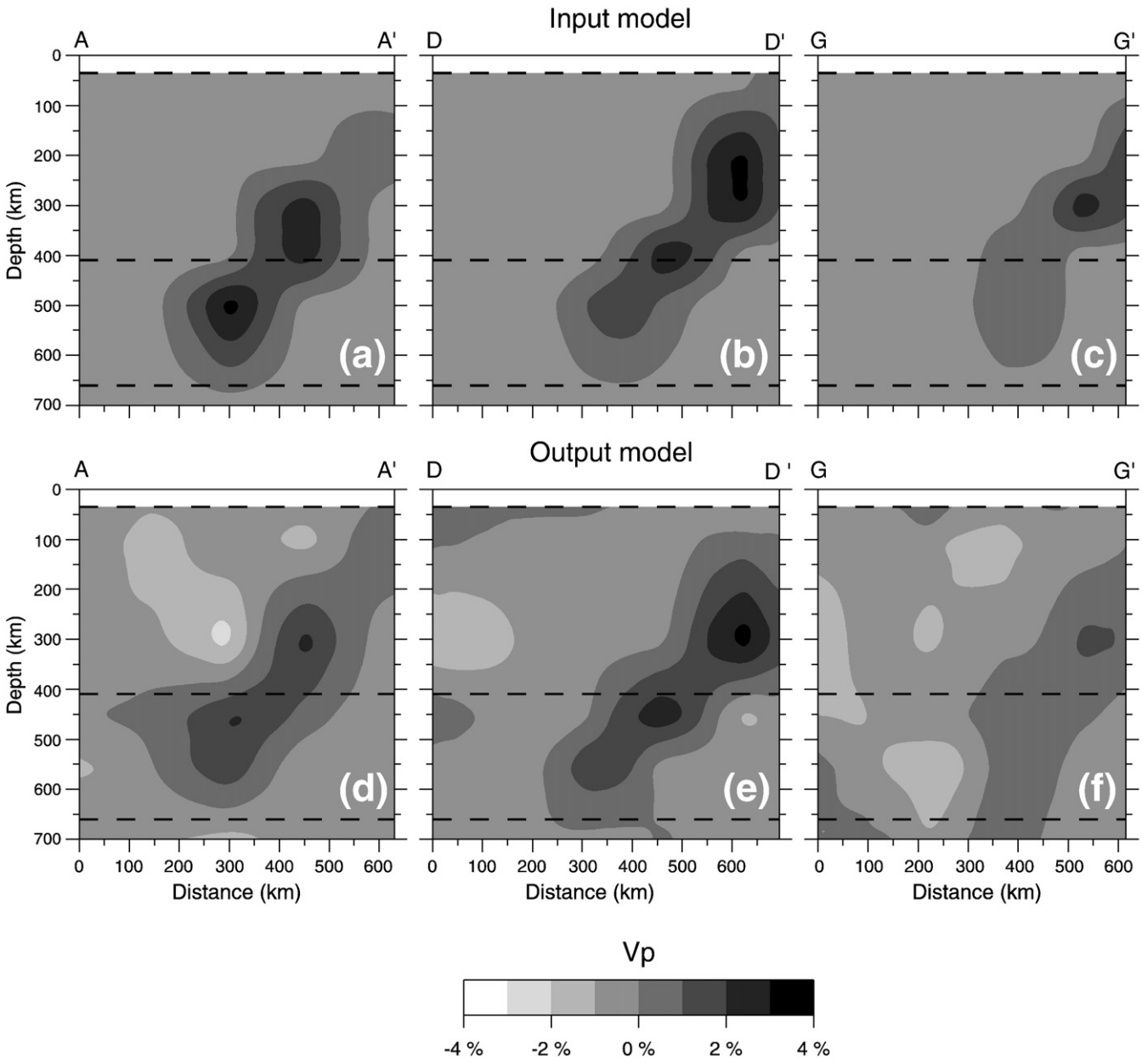

Fig. 12. Results of a synthetic resolution test. Locations of the profiles are shown in Fig. 9. (a–c) Input models; (d–f) inverted results. White and black colors represent slow and fast velocities, respectively. The velocity perturbation scale is shown at the bottom.

conducted to simulate the loss of a descending slab through the mantle, which suggests a significant displacement of asthenosphere beneath the slab as well as around it laterally (Buttles and Olson, 1998). From our model, we can see that the loss of slab mainly occurred where the Meiji seamounts exist. Davaille and Lees (2004) suggested that the presence of the Meiji seamounts provides accelerated partial melt that can account for the missing slab in the north. Therefore, the thermal friction by the mantle flow and the presence of Meiji seamounts jointly cause the diminishment of slab near the edge.

In addition to the main features of the high-V anomaly as mentioned above, there are two other high-V zones which should be mentioned although the resolution is not very high there. One is visible beneath the Bering Sea near the Aleutian–Kamchatka junction (Fig. 8), which may be the subducted Pacific plate along the Aleutian trench. The other high-V zone extends to northern Kamchatka at 700 km depth (Fig. 8f), which may be related to the tectonic evolution of Kamchatka. In the late Cenozoic, the Komandorsky plate subducting in northern Kamchatka may have weakened or stalled for 10 million years after the Komandorsky spreading (Baranov et al., 1991). Hochstaedler et al. (1994) found the adakites from the inactive volcanic centers in northern Kamchatka, which indicates the partial melts of the subducted oceanic crust. Combining shear-wave tomography with other geophysical and geological evidence, Levin et al. (2002a) suggested that a relict slab detached from the westward subduction of the Komandorsky basin lithosphere at 5 Ma or 10 Ma ago. Therefore, we consider that the high-V anomaly at 700 km depth may be the detached lithosphere of the spreading Komandorsky basin.

How did the gap near the slab edge affect the tectonics in Kamchatka? Near the Aleutian–Kamchatka junction, the Meiji seamounts, as a coincident event, subducted beneath Kamchatka at about 54°N accompanying the Pacific plate. Thermal modeling in Kamchatka shows the Pacific lithosphere beneath the Meiji–Hawaiian

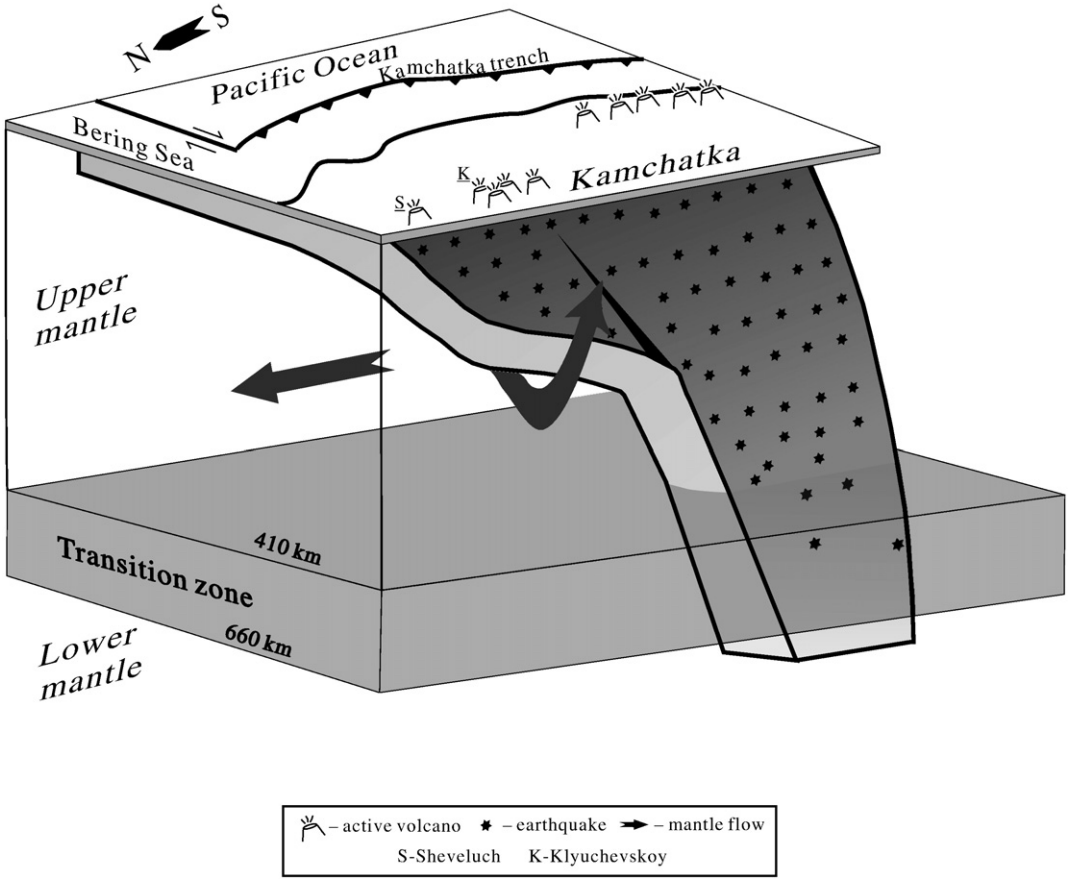

Fig. 13. Perspective image showing the Pacific plate subducting to the west through the mantle transition zone beneath Kamchatka (modified from Yogodzinski et al., 2001; Levin et al., 2002a). The uppermost thin board represents the crust. Asterisks indicate the seismicity (schematically) which shoal to the north beneath Kamchatka. Other symbols are shown at the bottom.

hotspot was already thinner well due to delayed thickening before entering the trench (Davaille and Lees, 2004). Owing to the influences of the Meiji seamounts and the slab loss, the remnant Pacific slab near the junction is less dense and has less negative buoyancy, and so should have a lower dip angle under northern Kamchatka (Fig. 13), as has been observed for other island seamount chains subduction (e.g., DeLong and Fox, 1977; Molnar and Atwater, 1978). As a result, this subduction with a lower dip angle has induced the Sheveluch and Klyuchevskoy volcanoes to shift westward.

Although we have only used teleseismic data recorded by 16 seismic stations in this study, the main features of the subducted Pacific slab under Kamchatka are revealed. In future studies, arrival time data from local earthquakes and teleseismic events may be used simultaneously, which would result in a much better tomography under Kamchatka, greatly improving our understanding of the geodynamic processes under the plate edge region.

6. Conclusions

To understand the deep structure and dynamics beneath the Kamchatka peninsula, we applied a 3-D teleseismic tomography method to P-wave arrival time data collected from digital seismograms of 75 teleseismic events released by the IRIS data center. Our results show that a high-V zone associated with the subducted Pacific slab extends below the transition zone and beyond the leading edge of the Wadati–Benioff zone under southern Kamchatka and it shoals northward and terminates near the Aleutian–Kamchatka junction, which is consistent with the pattern of seismicity and with the previous geophysical and geochemical studies. Our tomographic images also show low-V anomalies beneath northern Kamchatka and the Aleutian–Kamchatka junction that correspond to the asthenospheric flow.

Based on the present tomography results, we propose a gap model to interpret the loss of slab under northern Kamchatka. The gap caused by the slab loss may be generated by the thermal friction as the Pacific plate rotated clockwise at about 30 Ma ago, and be further enlarged by the slab-edge pinch-off of the asthenospheric flow and the presence of Meiji seamounts. Due to the less dense of Meiji seamounts and the slab loss, the Pacific plate subducts under northern Kamchatka with a lower dip angle, which caused the Sheveluch and Klyuchevskoy volcanoes to shift westward.

Acknowledgments

We thank the IRIS data center for providing the waveform data used in this study. We are grateful to Prof. Tom Parsons and two anonymous reviewers for providing constructive comments and suggestions that improved the manuscript. This work was partially supported by a research grant (Kiban-A 17204037) to D. Zhao from the Japanese Ministry of Education and Science. Most figures are made by using GMT (Wessel and Smith, 1998).

References

Baranov, B.V., Seliverstov, N.I., Muravev, A.V., Muzurov, E.L., 1991. The Komandorsky Basin as a product of spreading behind a transform plate boundary. Tectonophysics 199, 237–269.

Bazhenov, M.L., Burtman, V.S., Krezhovskikh, O.A., Shapiro, M.N., 1991. Paleotectonic reconstruction of the Aleutian Arc–Kamchatka convergence zone. Geotectonics 25, 244–256.

Braitseva, O.A., Melekestsev, I.V., Ponomareva, V.V., Sulerzhitsky, L.D., 1995. Ages of calderas, large explosive craters and active volcanoes in the Kurile–Kamchatka region, Russia. Bull. Volcanol. 57, 383–402.
Buttles, J., Olson, P., 1998. A laboratory model of subduction zone anisotrophy. Earth Planet. Sci. Lett. 164, 245–262.
Davaille, A., Lees, M., 2004. Thermal modeling of subducted plates: tear and hotspot at the Kamchatka corner. Earth Planet. Sci. Lett. 226, 293–304.
DeLong, S.E., Fox, P., 1977. Geological consequences of ridge subduction. In: Talwani, M., Pitman III, W.C. (Eds.), Island Arcs, Deep Sea Trenches, and Back-arc Basins. Maurice Ewing Ser., vol. 1. AGU, Washington, D.C., pp. 115–122.
DeMets, C., Gordon, R.G., Argus, D.F., Stein, S., 1990. Current plate motions. Geophys. J. Int. 101, 425–478.
Engdahl, E., van der Hilst, R., Buland, R., 1998. Global teleseismic earthquake location with improved travel times and procedure for depth determination. Bull. Seismol. Soc. Am. 88, 722–743.
Gorbatov, A., Kostoglodov, V., Suárez, G., 1997. Seismicity and structure of the Kamchatka subdunction zone. J. Geophys. Res. 102, 17883–17898.
Gorbatov, A., Domínguez, J., Suárez, G., Kostoglodov, V., Zhao, D., 1999. Tomographic imaging of the P-wave velocity structure beneath the Kamchatka peninsula. Geophys. J. Int. 137, 269–279.
Gorbatov, A., Widiyantoro, S., Fukao, Y., Gordeev, E., 2000. Signature of remnant slabs in the North Pacific from P-wave tomography. Geophys. J. Int. 142, 27–36.
Gordon, R.G., Jurdy, D.N., 1986. Cenozoic global plate motions. J. Geophys. Res. 91, 12389–12406.
Hochstaedler, A.G., Kepezhinskas, P.K., Defant, M.J., Drummond, M.S., Bellon, H., 1994. On the tectonic significance of arc volcanism in northern Kamchatka. J. Geol. 102, 639–654.
Honthaas, C., Bellon, H., Kepezhinskas, P.K., Maury, R.C., 1995. New ^{40}K–^{40}Ar dates for the Cretaceous–Quaternary magmatism of Northern Kamchatka (Russia). C. R. Acad. Sci. Paris Serie II 320, 197–204.
Humphreys, E., Clayton, R.W., 1988. Adaptation of back projection tomography to seismic travel time problems. J. Geophys. Res. 93, 1073–1085.
Kennett, B., Engdahl, E., 1991. Traveltimes for global earthquake location and phase identification. Geophys. J. Int. 105, 429–465.
Kimura, G., 1994. The latest Cretaceous–early Paleogene rapid growth of accretionary complex and exhumation of high pressure series metamorphic rocks in northwestern Pacific margin. J. Geophys. Res. 99, 22147–22164.
Lallemand, S.E., Font, Y., Bijwaard, H., Kao, H., 2001. New insights on 3-D plates interaction near Taiwan from tomography and tectonic implications. Tectonophysics 335, 229–253.
Laske, G., Masters, G., Reif, C., CRUST2.0: a new global crustal model at 2×2 degrees. http://mahi.ucsd.edu/Gabi/rem.dir/crust/crust2.html.
Lees, J.M., Brandon, M., Park, J., Levin, V., 2000. Kamchatka: edge of the plate. IRIS Newsl. 1, 17–19.
Lees, J.M., VanDecar, J., Gordeev, E., Ozerov, A., Brandon, M., Park, J., Levin, V., 2007. Three dimensional images of the Kamchatka-Pacific plate cusp. In: Eichedlberger, J., Gordeev, E., Kasahara, M., Izbekov, P., Lees, J.M. (Eds.), Volcanism and Subduction: The Kamchatka Region. AGU, Washington, D.C., pp. 65–75.
Lei, J., Zhao, D., 2005. P-wave tomography and origin of the Changbai intraplate volcano in Northeast Asia. Tectonophysics 397, 281–295.
Levin, V., Shapiro, N., Park, J., Ritzwoller, M., 2002a. Seismic evidence for catastrophic slab loss beneath Kamchatka. Nature 418, 763–767.
Levin, V., Park, J., Brandon, M., Lees, J., Peyton, V., Gordeev, E., Ozerov, A., 2002b. Crust and upper mantle of Kamchatka from teleseimic receiver function. Tectonophysics 358, 233–265.
Lucente, F.P., Chiarabba, C., Cimini, G.B., Giardini, D., 1999. Tomographic constraints on the geodynamic evolution of the Italian region. J. Geophys. Res. 104, 20307–20327.
Molnar, P., Atwater, T., 1978. Interarc spreading and cordilleran tectonics as alternates related to the age of subducted oceanic lithosphere. Earth Planet. Sci. Lett. 41, 330–340.
Montelli, R., Nolet, G., Dahlen, F.A., Masters, G., 2006. A catalogue of deep mantle plumes: new results from finite-frequency tomography. Geochem. Geophys. Geosyst. 7, Q11007. doi:10.1029/2006GC001248.
Mooney, W., Laske, G., Masters, G., 1998. CRUST5.1: a global crustal model at 5×5 degrees. J. Geophys. Res. 103, 727–747.
Nizkous, I., Sanina, I.A., Kissling, E., Gontovaya, L.I., 2006. Velocity properties of the lithosphere in the Ocean–Continent Transition Zone in the Kamchatka region from seismic tomography data. Phys. Solid Earth 42, 18–29.
Paige, C., Saunders, M., 1982. LSQR: an algorithm for sparse linear equations and sparse least squares. ACM Trans. Math. Softw. 8, 43–71.
Park, J., Levin, V., Brandon, M., Lees, J., Peyton, V., Gordeev, E., Ozerov, A., 2002. A dangling slab, amplified arc volcanism, mantle flow and seismic anisotrophy in the Kamchatka plate corner. Geodyn. Ser. 30, 295–324. doi:10/1029/030GD18.
Peyton, V., Levin, V., Park, J., Brandon, M., Lees, J., 2001. Mantle flow at a slab edge: seismic anisotrophy in the Kamchatka region. Geophys. Res. Lett. 28, 379–382.
Portnyagin, M., Hoernle, K., Avdeiko, G., Hauff, F., Werner, R., Bindeman, I., Uspensky, V., Garbe-Schönberg, D., 2005. Transition from arc to oceanic magmatism at the Kamchatka–Aleutian junction. Geology 33, 25–28.
Steblov, G.M., Kogan, M.G., King, R.W., Scholz, C.H., Bürgmann, R., Frolov, D.I., 2003. Imprint of the North American plate in Siberia revealed by GPS. Geophys. Res. Lett. 30. doi:10.1029/2003GL017805.
Watson, B.F., Fujita, K., 1985. Tectonic evolution of Kamchatka and Sea of Okhotsk and implication for the pacific basin. In: Howell, D.G. (Ed.), Tectonostratigraphic Terranes of the Circum-Pacific Region. Circum-Pacific Counsil, Houston, TX, pp. 333–348.
Wessel, P., Smith, W.H., 1998. New, improved version of the generic mapping tools released. Eos Trans., AGU 79. doi:10.1029/98EO00426.
Wortel, M.J.R., Spakman, W., 2000. Subduction and slab detachment in the Mediterranean–Carpathian region. Science 290, 1910–1917.
Yogodzinski, G.M., Lees, J.M., Churikova, T.G., Dorendorf, F., Wöerner, G., Volynets, O.N., 2001. Geochemical evidence for the melting of subucting oceanic lithosphere at plate edges. Nature 409, 500–504.
Zhao, D., 2001. Seismic structure and origin of hotspot and mantle plumes. Earth Planet. Sci. Lett. 192, 251–265.
Zhao, D., 2004. Global tomographic images of mantle plumes and subducting slabs: insights into deep Earth dynamics. Phys. Earth Planet. Inter. 146, 3–34.
Zhao, D., Hasegawa, A., Horiuchi, S., 1992. Tomographic imaging of P and S wave velocity structure beneath northeastern Japan. J. Geophys. Res. 97, 19909–19928.
Zhao, D., Hasegawa, A., Kanamori, H., 1994. Deep structure of Japan subduction zone as derived from local, regional, and teleseismic events. J. Geophys. Res. 99, 22313–22329.
Zhao, D., Lei, J., Inoue, T., Yamada, A., Gao, S., 2006. Deep structure and origin of the Baikal rift zone. Earth Planet. Sci. Lett. 243, 681–691.